Eur. Phys. J. E (2014) **37**: 18
DOI 10.1140/epje/i2014-14018-1

THE EUROPEAN PHYSICAL JOURNAL E

Regular Article

Self-consistent field theory of block copolymers on a general curved surface

Jianfeng Li[a], Hongdong Zhang, and Feng Qiu

The State Key Laboratory of Molecular Engineering of Polymers, Department of Macromolecular Science, Fudan University, Shanghai 200433, China

Received 20 July 2013 and Received in final form 17 December 2013
Published online: 26 March 2014 –

Abstract. In this work, we propose a theoretical framework based on the self-consistent field theory (SCFT) for the study of self-assembling block copolymers on a general curved surface. Relevant numerical algorithms are also developed. To demonstrate the power of the approach, we calculate the self-assembled patterns of diblock copolymers on three distinct curved surfaces with different genus. We specially study the geometrical effects of curved surfaces on the conformation of polymer chains as well as on the pattern formation of block copolymers. By carefully examining the diffusion equation of the propagator on curved surfaces, it is predicted that Gaussian chains are completely unaware of the extrinsic curvature but that they will respond to the intrinsic curvature of the surface. This theoretical assertion is consistent with our SCFT simulations of block copolymers on general curved surfaces.

1 Introduction

The microphase separation of block copolymers under various types of geometrical confinements (*e.g.* in the bulk phase or on surfaces) has attracted tremendous attention in the last decades. Many novel patterns of block copolymer emerge from rearrangements of the traditional ordered phases when adapting to these restrictions [1,2]. For instance, spiral patterns have been observed to occur in the cylindrical pore both in experiments and in theory [3–7]. The physics behind this space-confinement effect on the self-assembly of block copolymers has been clarified in Yu *et al.*'s work [2], where they revealed that the origin of these novel structures was the confinement-induced structural frustration characterized by the ratio between the pore size and the period of the structures. Block copolymers in other confinements, such as spherical pores, ellipsoidal pores or soft confinement, have also been investigated theoretically and exhibit rich morphologies [8–12]. However, the curvature effects on the self-assembled pattern formation of block copolymers confined to a curved surface are still far from being fully understood, although several theoretical works have been devoted to this problem [13–15]. The main obstacle may be that we still lack a general theoretical framework that can properly describe the microphase separation of block copolymers on a general curved surface.

On the other hand, self-consistent field theory (SCFT) [16] is well established for the study of the self-assembling of block copolymers. It has successfully predicted a variety of ordered bulk phases that have been observed in experiments, *e.g.*, lamella, hexagonal cylinder, sphere and gyroid order phases of diblock copolymers [16,17], and many intricate ordered phases of triblock copolymers [18,19]. However, it is a highly challenging and painful task to extend SCFT from flat space to curved surfaces, mostly due to the technical problems involved in numerically solving the relevant SCFT equations.

There are mainly three different types of numerical implementations [16] of SCFT in flat space (2D or 3D). The first one, the spectral screen method, was introduced by Matsen [17], where the SCFT fields and variables are spanned in reciprocal space [20]. In the second and third ones, the SCFT equations are both solved in real space [16,21,22]; the main difference between them is in the way of solving one of the SCFT equations: the diffusion equations of the propagator [23]. In the second implementation (pseudo-spectral method), the equation is solved using Fourier transformation; while in the third one, the equation is solved using alternative discrete implicit (ADI) schemes, such as the Crank-Nickson scheme [24] for 2D flat space. These three implementations work well in flat space; but they all encounter problems for curved surfaces. For the spectral or pseudo-spectral methods, there are no such base functions spanned on a general curved surface. For the latter, previous ADI schemes are all limited to flat space. Nevertheless, for the simplest curved surface (*i.e.* the spherical surface), the last two implementations have been successfully extended to this constant-Gaussian-curvature surface. In

[a] e-mail: lijf@fudan.edu.cn

2006, we designed a spherical ADI scheme and studied the microphase patterns of diblock and triblock copolymers on a sphere [14]. One year later, Chantawansri *et al.* [15] solved the diffusion equation on a sphere using the pseudo-spectral method and systematically studied the influences of sphere size on the assembled patterns of diblock copolymers. Some other numerical schemes have also been developed to deal with complex geometries. For instance, Kim *et al.* [25] have studied the steric interaction between two polymer-grafted particles using SCFT with a multiple-coordinate numerical scheme. In order to investigate the behaviors of block copolymers grafted to a sphere, Vorselaars *et al.* [26] developed a hybrid numerical scheme that combined a spherical-harmonics expansion for the angular coordinates with a modified real-space Crank-Nicolson method for the radial direction to solve the SCFT equations.

In experiments, however, nanoparticles usually exhibit a variety of shapes and topologies other than just spheres. The substrate that is used to support polymer films (or polymer melts) can also be curved [27]. Therefore, in order to explain these experiments, we need to develop a general theoretical framework based on SCFT that can properly describe the microphase separation of copolymers on a general curved surface, which will be the main focus of this article. In addition, we hope that the simulation results from the curved-surface SCFT (CSSCFT) can help understand some basic physics behind the curvature effects on the formation of these morphologies. We are especially interested in the influence of the intrinsic curvature (Gaussian curvature) on the self-assembly of block copolymers, which does not manifest for the spherical-surface case since the Gaussian curvature of the spherical surface is constant.

The article is organized as follows. In the Methodology section, we develop a general self-consistent field theory of diblock copolymers on curved surfaces. Numerical implementations of this curved-surface SCFT (CSSCFT) for a general curved surface using the triangulation representation and a quasi-flat surface using the Monge representation are both presented. In particular, CSSCFT for a general curved surface is an extension of our previous spherical ADI scheme [14]. In the Results section, we will first validate our method and demonstrate its effectiveness; then, a series of SCFT simulations will be carried out to reveal the influences of the curved surface on the microphase separation of block copolymers.

2 Theory and methodology

2.1 SCFT on a general curved surface

Consider n AB diblock copolymers with the polymerization of N confined on a curved surface $\mathbf{R}(u^1, u^2)$ parameterized by u^1 and u^2 with a total area S. The volume fraction of A block is f and the two blocks disfavor with each other characterized by the Flory-Huggins parameter χ. Then the free energy density of this system in the unit of k_BT can be written as

$$\frac{F}{nk_BT} = -\log\frac{Q}{S} + \frac{1}{S}\int[\chi N\phi_A\phi_B - \omega_A\phi_A - \omega_B\phi_B - \xi(1-\phi_A-\phi_B)]\mathrm{d}A, \quad (1)$$

by introducing two auxiliary fields ω_A and ω_B. In the above equation, Q is the partition function of a single AB block copolymer, $\phi_A(u^1, u^2)$ and $\phi_B(u^1, u^2)$ are A/B monomer densities, and $\xi(u^1, u^2)$ is another auxiliary field that is used to achieve the local incompressibility of the A/B segments. $\mathrm{d}A = \sqrt{g}\mathrm{d}u^1\,\mathrm{d}u^2$ is the area element of the surface with g the determinant of the metric tensor $g_{\alpha\beta} \equiv (\partial\mathbf{R}/\partial u^\alpha)(\partial\mathbf{R}/\partial u^\beta)$ of the surface with $\{\alpha, \beta\} \in \{1, 2\}$.

In SCFT, the single-chain partition function can be further expressed as $Q = \int q(u^1, u^2, s)q\dagger(u^1, u^2, s)\mathrm{d}A$ in terms of the end-segment distribution function (or the propagator) q and its conjugate $q\dagger$, which satisfy [28]

$$\frac{\partial q}{\partial s} = \frac{Na^2}{6}\nabla^2_{LB}q - \omega q,$$
$$\frac{\partial q\dagger}{\partial s} = -\frac{Na^2}{6}\nabla^2_{LB}q\dagger + \omega q\dagger, \quad (2)$$

where $s = 0 \sim 1$ is used to parametrize the polymer chain. $\omega = \omega_A$ for $s \le f$ while $\omega = \omega_B$ for $s > f$. ∇^2_{LB} is the Laplace-Beltrami operator which is actually the divergence operator for the curved surface and can be expressed, in terms of metric tensors, as $\nabla^2_{LB} = \frac{1}{g^{1/2}}\frac{\partial}{\partial u^\alpha}[g^{1/2}g^{\alpha\beta}\frac{\partial}{\partial u^\beta}]$ where the Einstein summation rule is applied. Initial conditions are $q(u^1, u^2, 0) = 1$ and $q\dagger(u^1, u^2, 1) = 1$. (According to our recent theory (not published) about the diffusion equation of the prapogator of Gaussian chains on curved surfaces, there should be an extra term in the field ω: *i.e.* $\omega \to w + Na^2K/9$ with K the Gaussian curvature. But in the current study, this extra term can be absorbed into the field ξ and be safely neglected, since it only depends on the position. If Kuhn lengths of A/B blocks are different, then this extra term will be important. We will investigate this case in our future study.)

Minimization of the free energy with respect to the five fields $\phi_{A/B}$, $\omega_{A/B}$ and ξ leads to the five SCFT equations

$$\omega_A = \chi N\phi_B - \xi, \quad (3)$$
$$\omega_B = \chi N\phi_A - \xi, \quad (4)$$
$$\phi_A = \frac{S\int_0^f q(u^1, u^2, s)q\dagger(u^1, u^2, s)\mathrm{d}s}{Q}, \quad (5)$$
$$\phi_B = \frac{S\int_f^1 q(u^1, u^2, s)q\dagger(u^1, u^2, s)\mathrm{d}s}{Q}, \quad (6)$$
$$1 - \phi_A - \phi_B = 0, \quad (7)$$

where S is the total area of the curved surface. These five equations, together with the diffusion equations and the expression for Q, form a complete set of the SCFT

equations. Except for the diffusion equations, other SCFT equations are basically the same as those in flat space; or in other words, the curved-surface effect comes in the curved-surface SCFT only in terms of the Laplace-Beltrami operator occurred in the diffusion equations.

In what follows, we shall carefully examine, in theory, the above diffusion equations in order to investigate the curvature effects on the self-assembly of polymers. The primary conclusion is that the block copolymers modelled as Gaussian chains are "unaware" of the extrinsic curvature but will respond to the intrinsic curvature of the surface. The explanations or the proof are given as follows. i) *Intrinsic curvature* (referred to as *Gaussian curvature* for a 2D surface) is the curvature that can be completely determined by the measurements of distance within the surface or by the metric tensors and does not depend on how the surface is embedded in a higher dimensional space; while, on the other hand, the *extrinsic curvature* (usually referred to as *mean curvature* for a 2D surface) does depend on details of the embedding ways. One important geometrical fact about these two types of curvature is that the intrinsic curvature is invariant under an isometric transformation, which is a transformation that preserves the metric, while the extrinsic curvature can be changed by an isometric transformation. ii) Actually, any quantity that can be expressed purely in terms of the metric will be invariant under an isometric transformation. iii) All quantities in the above SCFT equations can be expressed purely in terms of the metric tensor including the Laplace-Beltrami operator, so the self-assembly of block copolymers described by these equations will be invariant under isometric transformations. According to i), one can say that the self-assembly of Gaussian chains on curved surfaces is "unaware" of the extrinsic curvature of the surface but will respond to the intrinsic curvature. This theoretical prediction will be tested in sect. 3.3 by our SCFT simulations.

We may also want to examine, in theory, the way of the block copolymers modelled as Gaussian chains respond to Gaussian curvature locally. The basic idea is to "subtract" the planar Laplacian operator from the non-planar Laplacian operator, *i.e.* Laplace-Beltrami, to see the connection between the remaining terms and the Gaussian curvature. To simplify the situation, we only consider a small neighboring area of a point $\mathbf{r}_0$ on the surface and draw a small geodesic circle around that point, where the geodesic distances on the circle to the point are all equal to r. The q value on $\mathbf{r}_0$ is denoted as q_0 while the q value on the circle is denoted by q_r. According to Stokes' theorem, the divergence of q at $\mathbf{r}_0$ is approximated as

$$\nabla^2_{LB} q \approx \frac{\oint \frac{q_r - q_0}{r} \mathrm{d}l}{A(r)}, \tag{8}$$

where the integration is over the geodesic circle and $A(r)$ is the area of the geodesic circle.

By noting the Bertrand-Diquet-Puiseux theorem [29], we have

$$K \approx \frac{12(\pi r^2 - A(r))}{\pi r^4} \tag{9}$$

and

$$K \approx \frac{3(2\pi r - C(r))}{\pi r^3}, \tag{10}$$

where $K = c_1 c_2$ is the Gaussian curvature and $c_{1,2}$ are the two principal curvatures at the point $\mathbf{r}_0$, and $C(r) = \oint \mathrm{d}l$ is the circumference of the geodesic circle. Therefore, $A(r)$ and $C(r)$ can be expressed as

$$A(r) \approx \pi r^2 \left(1 - \frac{Kr^2}{12}\right) \tag{11}$$

and

$$C(r) \approx 2\pi r \left(1 - \frac{Kr^2}{6}\right). \tag{12}$$

Plugging these two equations back in eq. (8), the Laplace-Beltrami operator can be re-expressed, to the order of Kr^2, as

$$\begin{aligned} \nabla^2_{LB} q &\approx \frac{(1 - \frac{Kr^2}{6})^2}{(1 - \frac{Kr^2}{12})} \nabla^2_{fl} q \\ &= \left(1 - \frac{Kr^2}{4} + O(K^2 r^4)\right) \nabla^2_{fl} q, \end{aligned} \tag{13}$$

where

$$\nabla^2_{fl} q = \frac{\oint \frac{q_r - q_0}{r} \mathrm{d}l}{\pi (\frac{C(r)}{2\pi})^2} \tag{14}$$

should be seen as the divergence on the flat surface.

Plugging eq. (13) back into the diffusion equation leads to

$$\frac{\partial q}{\partial s} = \frac{Na^2}{6} \nabla^2_{fl} q - \left[\omega + \frac{Na^2 K r^2}{24} \frac{\nabla^2_{fl} q}{q}\right] q. \tag{15}$$

This shows that polymers are affected by an extra field $\frac{Na^2 Kr^2}{24} \frac{\nabla^2_{fl} q}{q}$ because of the Gaussian curvature. In addition, this extra field cannot be absorbed into the field ξ because $\nabla^2_{fl} q$ in the expression not only depends on the position but also depends on the species of the A/B blocks. For an A-dominant spot pattern on a peak of a quasi-flat surface (fig. 11), K is positive and $\nabla^2_{fl} q$ is negative for $s \in [0, f]$, therefore the extra field for A-segment is negative, which means the A-segment tends to stay on the peak. This phenomenon can be also seen in our simulations of the patterns of block copolymers on a quasi-flat surface (fig. 11).

2.2 Numerical implementations

As discussed in the Introduction section, the main problem of extension of SCFT to curved surfaces is to find an effective numerical scheme to solve the diffusion equation (eq. (2)).

In the real-space implementation of SCFT in 2D space, the diffusion equation can be solved numerically using an implicit scheme; the implicit scheme reads $[q(x, y, s+\Delta s) - q(x, y, s)]/\Delta s = (L_x + L_y - \omega)[q(x, y, s+\Delta s) + q(x, y, s)]/2$,

where $L_x q(x,y) \equiv \frac{Na^2}{6\Delta x^2}[q(x+\Delta x,y)+q(x-\Delta x,y)-2q(x,y)]$ is the discrete form of $\partial^2/\partial x^2$ that has adsorbed the prefactor $Na^2/6$; L_y is defined similarly. However, this scheme is computationally expensive. To reduce the cost, an alternative direction implicit (ADI) scheme, the Crank-Nicolson algorithm [24], is usually applied. The basic idea of ADI is to split the discrete Laplacian $L_x + L_y$ into L_x and L_y, and the corresponding implicit scheme can also be split into the following two equations:

$$\begin{aligned}
&\left(1-\frac{\Delta s}{2}L_x+\frac{\Delta S}{4}\omega\right)q* = \\
&\left(1+\frac{\Delta s}{2}L_y-\frac{\Delta S}{4}\omega\right)q(x,y,s), \\
&\left(1-\frac{\Delta s}{2}L_y+\frac{\Delta S}{4}\omega\right)q(x,y,s+\Delta s) = \\
&\left(1+\frac{\Delta s}{2}L_x-\frac{\Delta S}{4}\omega\right)q*, \qquad (16)
\end{aligned}$$

where $q*$ is merely the intermediate quantity that can be eliminated by adding the two equations together after multiplying the first of the above equations by $(1+\frac{\Delta s}{2}L_x-\frac{\Delta S}{4}\omega)$ and the second by $(1-\frac{\Delta s}{2}L_x+\frac{\Delta S}{4}\omega)$, respectively. By this elimination, the above equations can be reduced to an ordinary implicit scheme to the accuracy of the second order of Δs (note that this inaccuracy might cause problems on the conservation of the polymer chains for big χN; this inaccuracy will be worse for the curved surface, which is one of the reasons why the ADI scheme cannot deal with large-χN cases). Now, solving the above equations only involves calculating the inverses of (cyclic) tridiagonal matrices which would be much simpler than tackling the ordinary matrices.

Basically, the central ideas of ADI are: i) Split the discrete Laplacian into different components. ii) Split the ordinary implicit scheme into several equations in order that each equation can be solved by evaluating a tridiagonal matrix (or a cyclic tridiagonal matrix for periodic boundary conditions). iii) These split equations can be transformed back into the former implicit scheme by eliminating the intermediate quantities.

In sects. 2.2.1 and 2.2.2, we will extend these ideas to numerically solve the diffusion equations on curved surfaces.

2.2.1 SCFT on a quasi-flat surface

Here, a quasi-flat surface is defined as a surface that is basically flat but with only some small bumps or small hills in it, in order that it can be cast in a Monge representation using the height function $h(x,y)$.

We assume that (x,y) has been discretized into square lattices with the spacing $\Delta x = \Delta y$ and we denote (x,y) as $(i\Delta x, j\Delta y)$ or simply as (i,j) with i and j two integers. Using Stokes' theorem, the discrete Laplacian operator

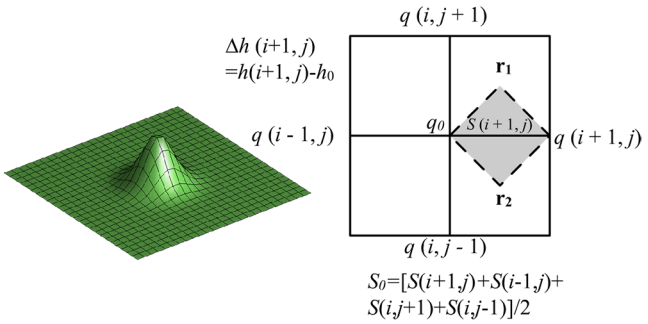

Fig. 1. The schematic illustrations of a quasi-flat surface and the discrete Laplacian operator for a quasi-flat surface. $\mathbf{r}_1$ and $\mathbf{r}_2$ (3D vectors) are two mass central points of their four neighboring lattice points, respectively. $S_0/2$ is the area element of the center point $(x,y,h(x,y))$. Δh is the height difference between two neighboring lattice points.

can be expressed as

$$\begin{aligned}
(L_x(x,y)+L_y(x,y))q_0 = &(q(i-1,j)-q_0)l_x(i,j,1) \\
&+(q(i+1,j)-q_0)l_x(i,j,2) \\
&+(q(i,j-1)-q_0)l_y(i,j,1) \\
&+(q(i,j+1)-q_0)l_y(i,j,2), \qquad (17)
\end{aligned}$$

where $L_x(x,y)q_0 \equiv (q(i-1,j)-q_0)l_x(i,j,1)+(q(i+1,j)-q_0)l_x(i,j,2)$, $l_x(i,j,1) = 2S(i-1)/S_0/(\Delta x^2+\Delta h^2(i-1,j))$, $l_x(i,j,2) = 2S(i+1)/S_0/(\Delta x^2+\Delta h^2(i+1,j))$ with $S_0 = [S(i+1,j)+S(i-1,j)+S(i,j+1)+S(i,j-1)]/2$; and $L_y(x,y)$, $l_y(i,j,1)$, $l_y(i,j,2)$ are defined similarly. The definitions of other variables can be seen in fig. 1. It is easy to check $h(x,y) = 0$ in a 2D flat space; when this occurs, the above expression is reduced to the ordinary discrete Laplacian operator.

Plugging this expression back into the Crank-Nicolson scheme (eq. (16)) leads to the ADI scheme for quasi-flat surfaces

$$\begin{aligned}
&\left(1-\frac{\Delta s}{2}L_x(x,y)+\frac{\Delta s}{4}\omega\right)q* = \\
&\left(1+\frac{\Delta s}{2}L_y(x,y)-\frac{\Delta s}{4}\omega\right)q(x,y,s), \\
&\left(1-\frac{\Delta s}{2}L_y(x,y)+\frac{\Delta s}{4}\omega\right)q(x,y,s+\Delta s) = \\
&\left(1+\frac{\Delta s}{2}L_x(x,y)-\frac{\Delta s}{4}\omega\right)q*, \qquad (18)
\end{aligned}$$

where $q*$ is the intermediate quantity. Note that the operators L_x and L_y depend on the position (i,j) as well as the height function $h(x,y)$ and the prefactor $Na^2/6$ has been absorbed into L_x and L_y.

2.2.2 SCFT on a general curved surface

However, not all surfaces can be represented using height functions and the closed surface of a spherical nano-

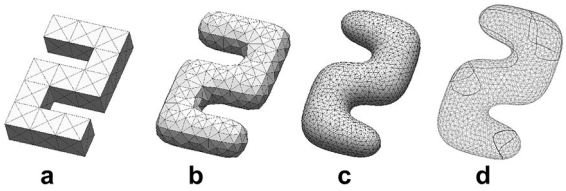

Fig. 2. The shape of the number "2" (c) with 2944 small triangles and 1474 vertices is generated from a "raw" shape (a) that is composed of eleven cubes using the Surface Evolver. (a) The shape "2" is formed by stacking 11 cubes together. (b) Refine the shape (a) once using the command "r" in the Evolver. The resulting shape is composed of 368 vertices. (c) Refine the shape (b) one more time. (d) The red curve and the black curve are two typical circular paths produced by our ADI scheme generating program.

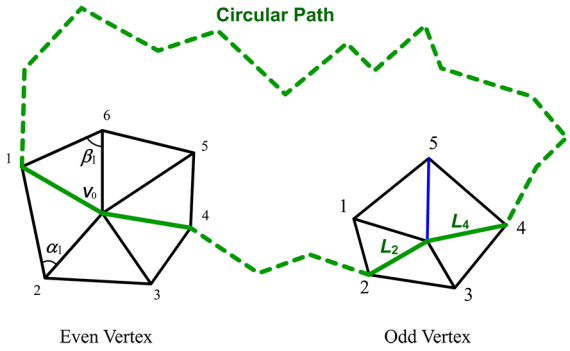

Fig. 3. The schematic illustration of the circular path on a triangulated mesh. The green dash and green solid lines form a circular path.

particle is such an example. In our previous work, we discretized the spherical surface with a triangulated mesh and designed a spherical ADI scheme to simulate the self-assembled patterns of diblock and triblock copolymers confined to the spherical surface. In this work, the spherical ADI scheme will be further extended to solve the diffusion equation on a general curved surface.

In the spherical ADI scheme, six circular paths, each with $L \times 5L$ lattices, are used to cover the sphere and the ADI equation is designed for each circular path. L is the width of the path. But for a general surface, there are no such regular paths that happen to cover the whole surface. However, we can still use the following ideas developed in the spherical ADI scheme. First, the ADI equation can only be solved along a *circular* path (or with some boundary condition). Second, at each vertex of the mesh, every direction (or component) of the discrete Laplacian operator should be covered at least once by the path (the meaning of the direction of the operator will be clear in the following context).

It is expected that the ADI scheme for a general curved surface will be highly complicated. In the following context, we shall present the relevant procedures step by step.

1) *Generating the initial curved surface.*– A general curved surface represented by a triangulated mesh can be constructed using a free piece of software called "Surface Evolver (SE)" by Brakke [30] or by any commercial 3D drawing software. For example, in fig. 2, the shape of the number "2" represented by a triangulated mesh is generated by the Evolver. The first shape (a) in fig. 2 is formed by stacking 11 cubes together. The data file for this shape can be composed by hand with the knowledge of the positions of the vertices and the relations between vertices, edges and faces. Specifically, three arrays are used to store the information of the triangulated mesh: $\mathbf{r}_k$ the positions of the vertices of the mesh with k labelling the vertex number, $[v_j^1, v_j^2]$ the two vertices of the edge j, and $[E_l^1, E_l^2, E_l^3]$ the three edges of the small triangle l. Then we refine the mesh by inserting a new vertex in the middle of each edge and creating the corresponding edges and small triangles related with the newly added vertices (in SE this can be done by entering the command "r"). By minimizing the bending energy of the refined surface we obtain fig. 2(b), which can be done by simply entering the "g" command in SE, and repeating these two processes yields fig. 2(c). We have ensured that the resultant triangulated mesh is smooth and there are no obtuse triangles on the mesh. This was done, because obtuse triangles might cause severe numerical problems for the discrete Laplace-Beltrami operator. Luckily, the obtuse triangles can be easily eliminated by the bond-flip operation (command "u"). In addition, the averaging operation (command "V") is commonly used to ensure that every triangle is roughly with the same size. We have shown that these surface operations are important for simulations of the deformations of multi-component vesicles [31].

2) *Evaluating the discrete Laplace-Beltrami operator.*– For a triangulated mesh of a curved surface, the corresponding discrete Laplace-Beltrami operator at each vertex of the mesh can be calculated based on the finite volume algorithm (or equivalently Stokes' theorem in discrete form) [13,14,32]. In fig. 3, for example the discrete Laplace-Beltrami (LB) operator on the lattice V_0 can be expressed as

$$\nabla^2_{LB} q = \frac{1}{2A_0} \sum_k (\cot \alpha_k + \cot \beta_k)(q_k - q_0) \equiv \sum_k L_k q_0, \tag{19}$$

where α_k and β_k are two angles opposite to the edges in two triangles sharing the edge $V_k V_0$, and $A_0 = \sum_k (\cot \alpha_k + \cot \beta_k) d_k^2/8$ is the area element of the lattice point V_0 with d_k the length of the edge $V_k V_0$. The summation is over the edges adjacent to the point V_0. L_k is one of the components of the discrete LB operator and we name it as the k-direction of the LB operator at the point V_0. Obviously, it is defined as

$$L_k q_0 = \frac{1}{2A_0} (\cot \alpha_k + \cot \beta_k)(q_k - q_0). \tag{20}$$

Note that we have not directly discretized the metric tensor g_{ij} to obtain the discrete form of the LB operator because it turns out that the corresponding scheme is

usually not compatible with the symmetry of the discrete mesh. But we emphasize that in the continuum limit the discrete scheme of eq. (19) derived from Stokes' theorem can be reduced to the continuous form of the LB operator in terms of metric tensors.

3) *Finding the circular paths.*– For simplicity, we can see a discrete lattice or mesh as a woven net. The ordinary implicit scheme treats the entire net as a whole; whereas the ADI scheme will first unweave the net thread by thread and then equations will be solved over each individual thread (or path). If the thread is not closed, then some boundary conditions are required for the two ends of the thread. For a closed surface represented by a triangulated mesh, it is expected that the net can be woven with a bunch of closed (or circular) threads; note that some edges of the small triangles in the triangulated mesh may be covered more than once by these threads. Our task here is to find a bunch of closed threads that can be used to weave a given triangulated mesh. In the following context, we shall call these closed threads circular paths for consistency. Certainly for an open surface, some paths will be open with the two ends touching the surface edge and some boundary conditions will be needed in this case.

Unlike the circular paths in the spherical ADI scheme where each path can be spanned on a $L \times 5L$ lattice of width L, the path in the curved-surface ADI scheme is actually a closed zig-zag curve with the width 1 (the green curve in fig. 3). To ensure that every direction of the Laplace-Beltrami (LB) operator on every vertex has been covered by some circular path(s), we employ the following procedures to find all paths. First, we randomly select a directed edge (each edge corresponds to a LB direction) that has not been covered by previous paths; for example, L_2 in fig. 3. Second, we count the number of the edges that are adjacent to the next vertex; if it is even we call it an *even* vertex, otherwise it is an *odd* vertex. Third, for an even vertex we select the edge that is "opposite" to the current edge. For example, for the vertex V_0 in fig. 3 the path should go from "1" to "V_0" to "4". For an odd vertex, there are two possible "opposite" edges. For example in fig. 3, the edge "2" in the odd vertex has two 'opposite' edges: "4" and "5". We choose one of them as the next edge for this path and another edge for the second time when we go through the edge "2"-"V_0" again. Fourth, continue until we come back to the initial edge or the coming edge touches the boundary edge of the surface, which indicates we have just finished finding a circular path (or a boundary-to-boundary path). Repeat the above four steps until all the LB directions of each vertex have been exhausted and a set of circular paths that can cover the whole surface can be obtained. Note that for a given triangulation mesh, there is probably more than one way of weaving the mesh.

4) *The ADI scheme on curved surface.*– Suppose we have found M circular paths on the curved surface that can fully cover all the edges of the mesh. For the vertex v on the mth circular path, the ADI scheme can be expressed as

$$\left(1 - \frac{L_L}{2} - \frac{L_R}{2} + \beta\omega\Delta s\right) q_v^m = \left(1 + \frac{L_L}{2} + \frac{L_R}{2} + \sum_{k=1}^{n_v-2} L_{Sk} + (\beta - 1)\omega\Delta s\right) q_v(s), \quad (21)$$

where $L_{L,R}$ are the LB directions of the vertex v that are lying on the mth path and L_{Sk} denotes other LB directions of vertex v. For instance, in fig. 3, if the path goes from "1" to "V_0" to "4", then $L_{L,R}$ at vertex "V_0" are L_1 and L_4, and L_{Sk} is referred to as L_2, L_3, L_5 and L_6. Notice that we have absorbed the prefactor $Na^2\Delta s/6$ into these LB operator components and their definitions can be read in eq. (19). n_v is the number of edges adjacent to v and $\beta = 1/n_v$. q_v^m is the intermediate quantity on path m. ω is the external field.

Suppose there are L_{path} vertices on the circular path m. Then we have L_{path} similar equations according to eq. (21). Putting them together, we can turn them into matrix form

$$T\mathbf{Q}_m = \mathbf{R}_m(s), \quad (22)$$

where T is a cyclic tridiagonal matrix with the non-vanishing entries of $T_{L_{\text{path}}1}$ and $T_{1L_{\text{path}}}$, $\mathbf{Q}_m = [q_{v_1}^m, q_{v_2}^m, \ldots, q_{v_{L\text{path}}}^m]^T$ and the elements of $\mathbf{R}_m(s)$ can be computed as the right-hand side of eq. (21). Note that there are M matrix equations of the same form as eq. (22) for M paths. By the Sherman-Morrison formula [33], the above equation can be easily reduced to compute the inverse of the ordinary tridiagonal matrix using the Thomas algorithm [24].

If all intermediate quantities q_v^m of all vertices on all paths have been worked out using eqs. (21) and (22), then $q_v(s + \Delta s)$ can be expressed as

$$q_v(s + \Delta s) = \frac{\sum_1^{N_p} \sum_1^{R_E} \frac{q_v^m}{R_E}}{N_p}, \quad (23)$$

where $N_p = n_v/2$ for an even vertex and $N_p = n_v$ for an odd vertex. R_E counts how many times an LB direction has been covered by the circular paths. Generally it will be only once, sometimes twice and rarely three times.

It is easy to check that, for a spherical surface, the above ADI scheme can be reduced to the spherical ADI scheme proposed by us in 2006 [14].

3 Results and discussions

3.1 Patterns on spheres with different discretizations

The method described in sect. 2.2.2 can be applied to any curved surface using triangulated representation. Therefore, it can also be applied to a spherical surface. In what follows, we re-construct the spherical ADI scheme from ref. [14] using our curved-surface-ADI-scheme generating program based on the procedures described in sect. 2.2.2. Then we demonstrate that the results do not depend too

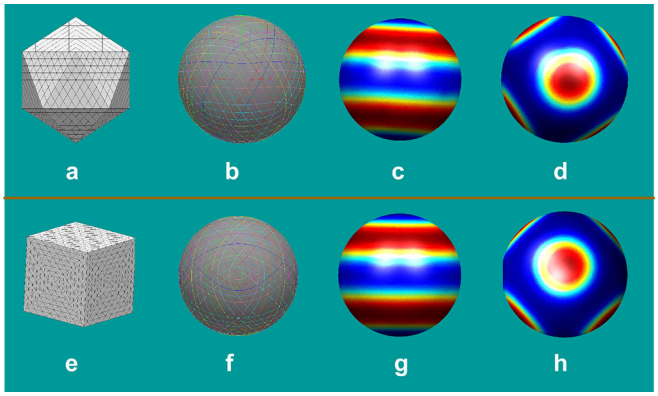

Fig. 4. The spherical ADI schemes for two different discretizations of a sphere and the corresponding diblock morphologies. (a)-(d) is for an icosahedron-based mesh and (e)-(h) for a cube-based mesh. (a) and (e) are an icosahedron and cube with refining triangulated mesh on them. (b) and (f) are the circular pathes obtained by our curved-surface ADI scheme. Edges along the same path are colored the same. (c) and (g) are striped patterns for both cases, where $f = 0.5$ and $\chi N = 13$. (d) and (h) are spotted patterns for both cases, where $f = 0.3$ and $\chi N = 15$. Red is for A block and Blue for B.

heavily on how the surface is discretized. The accuracy and efficiency of the method will also be discussed in this subsection.

As can be seen in fig. 4, the spherical surface can be discretized based on the icosahedron (which is the same as our previous work [14]) as well as based on a cube. The information about the circular paths obtained by our path searching program as well as the triangulations is listed in table 1. The circular paths can also be seen in fig. 4 where the edges on the same path have been stained with the same color. It is found that for the triangulation based on an icosahedron, if we gather all paths that are relatively parallel with each other together then they actually form a belt or path with width $L = 9$ and there are six of them exactly corresponding to the six paths (notice that $6 \times 9 = 54 = N_{\rm path}$) in the spherical ADI scheme [14]. Therefore, the spherical ADI scheme in ref. [14] is just one typical example of the general curved-surface ADI scheme.

It is exciting to find that the curved-surface ADI scheme can automatically generate the spherical ADI scheme for the triangulation based on a cube. It has 48 paths, each with 48 edges. Note that $N_{\rm path} \times L_{\rm path} = 48 \times 48 = 2304 = N_E$, which indicates that every edge is covered by the path only once in this ADI scheme. This also indicates that all the vertices in this mesh should be *even* vertices (all with six or four neighboring edges), while the ADI scheme for the icosahedron case has $54 \times 40 = 2160 > N_E = 1920$ which means some edges have been covered more than once. The reason for this is that there are twelve *odd* vertices, each with five neighboring edges in this triangulation.

In the two arrays of calculations (for the icosahedron and cube cases, respectively), we set the sphere radius to 7.32, the chain length $N = 50$, the Kuhn length $a = 1$, and $\chi N = 13$ for $f = 0.5$ and $\chi N = 15$ for $f = 0.3$; usually, the external field ω or free energy will converge to the accuracy of 10^{-6} within 1000 SCFT iterations for $\chi N \leq 25$ and the convergence rate of the free energy does not heavily depend on the discretization degree N_v. We obtain exactly the same striped and spotted patterns for both cases. As can be seen from fig. 4(c) and (g), A-blocks both form two circular stripes on the sphere, which looks like Jupiter; while in (d) and (h), the A-blocks both form six spots located on the vertices of an octahedron. The free energies of the patterns for the cube-based mesh (3.165379 for $f = 0.5$ and 2.725310 for $f = 0.3$) are only slightly smaller than those for the icosahedron-based mesh (3.165797 for $f = 0.5$ and 2.725621 for $f = 0.3$); the discrepancy is mostly due to the discretization degree of these two meshes ($N_v = 770$ for cube case *versus* $N_v = 640$ for icosahedron) rather than due to the type of discretization method. These results imply that the SCFT calculations are not sensitive to the triangulation as long as the discretization is reasonable (*i.e.* there are no obtuse triangles and none of the triangles within the mesh are too big or too small; smooth meshes work better, but are not mandatory). But note that, to achieve a sufficient accuracy of the SCFT calculation, it is recommended that the interaction parameter χ should not be too big ($\chi N < 25$) and the discretization degree (N_v) should ideally be bigger than 1000 (in this case, the above free-energy discrepancy can be reduced to about 5×10^{-5}).

Table 1. The information about the triangulations and the circular paths of two different representations of the spherical surface based on refining the icosahedron and the cube, respectively. N_v, N_E, N_F and $N_{\rm path}$ denote the number of vertices, edges, faces and pathes, respectively. R_0 is the radius of the sphere and $L_{\rm path}$ the length of the circular path indicating the number of edges on a single path.

	N_v	N_E	N_F	R_0	$N_{\rm path}$	$L_{\rm path}$
Icosahedron	642	1920	1280	7.23	54	40
Cube	770	2304	1536	7.23	48	48

In addition, the efficiency of the numerical scheme has also been investigated (see fig. 5 and fig. 6). Figure 5 shows that the computational time for a single SCFT iteration based on the ordinary implicit scheme obeys a cubic law; it is expected that it will be extremely time consuming when the discretization degree (N_v) is big. For instance, for $N_v = 642$ (the discretization degree of fig. 4b) $t = 2.616s$, but it quickly grows to be $49.11s$ for $N_v = 1912$ (the discretization degree for a cubic-frame surface in fig. 7). Figure 6, on the other hand, shows that the curved-surface ADI (CS-ADI) scheme can dramatically reduce the computation time. For instance, the computation time for a single SCFT iteration for the cubic-frame case drops to $1.6s$ when CS-ADI is employed, being about 30 times shorter than that for the ordinary implicit scheme. Furthermore, the average computation time depends roughly linearly on the discretization degree for a given type of mesh, though the slope of the dependence might depend on the complexity of the discretization. For example, the

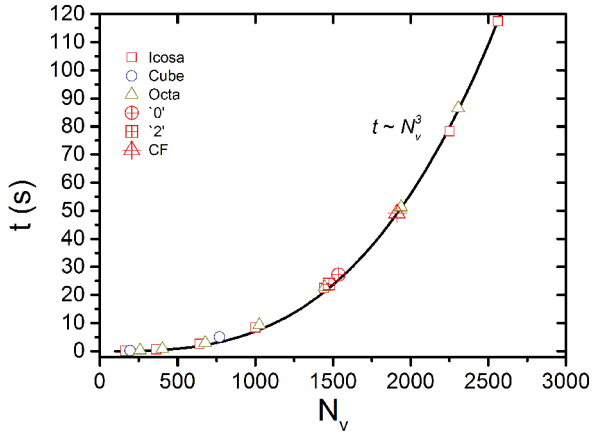

Fig. 5. The computation efficiencies of SCFT calculations based on the ordinary implicit scheme on six different curved meshes. "Icosa" stands for the spherical icosahedron-based mesh, 'cube' for the cube-based mesh and "octa" for the octahedron-based mesh; "0", "2" and "CF" are referred to as the three complex curved surfaces of fig. 7. All these data points are found to be quite close to the guiding black curve $t = (N_v/523)^3$, where t measures the average time (in the unit of second) required for a single SCFT iteration for different lattice number N_v. Note that an SCFT simulation requires about 1000 iterations. All calculations were performed on a personal computer equipped with an i7 CPU (2.0 GHz).

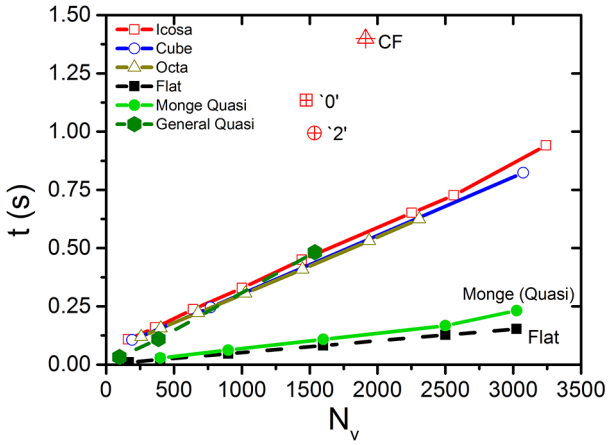

Fig. 6. The efficiencies of SCFT calculations for different ADI schemes in different situations. t measures the average time (in seconds) required for an SCFT iteration for different lattice number N_v. All these calculations were carried out on a personal computer equipped with an i7 CPU (2.0 GHz). "Flat" employs the ADI scheme eq. (16); "Monge (Quasi)" uses the ADI scheme eq. (18) with a quadrilateral lattice; "General Quasi" is also for a quasi-flat case but uses the curved-surface ADI scheme eqs. (21)–(23) with a triangular lattice. The other curves or data points all employ the curved-surface ADI scheme; in particular, "icosa", "cube" and "octa" are three different discretizations of a spherical surface based on refining the icosahedron, cube and octahedron, respectively. The three individual data points "2", "0" and "CF" describe the efficiency of the SCFT calculations on the three curved surfaces in fig. 7.

SCFT calculations on a spherical mesh are obviously more time-consuming (have a bigger slope) than those in a flat plane.

3.2 Patterns on surfaces with different genera

To further demonstrate the power of our curved-surface ADI scheme, we have carried out the SCFT calculations on the shapes of "2", "0" and a cube frame of genus 5. The geometries for these three shapes and the information for the corresponding triangulations are listed in table 2. The parameter setting is $\chi N = 13$ for $f = 0.5$ and $\chi N = 15$ for $f = 0.3$ with $N = 50$ and $a = 1$. As can be seen from fig. 7, we have successfully obtained patterns of block copolymers on these three closed surfaces with different genera.

Further more, the striped patterns of block copolymers shown in fig. 7 have the following three important features. First, on the same surface, the stripes tend to align roughly through the same direction even though sometimes there are "holes" in the surface. Second, the boundary interfaces between the A/B segments tend to be "straight" or mathematically they prefer to go along the geodesics of the surface, in order to reduce interface boundary energy. Third, the defects or spotted phases tend to form on the peaks of the shape where the Gaussian curvature is positive.

For spotted patterns, spots also prefer to stay at the peaks of the surface with the positive Gaussian curvature. Another interesting feature is that the elongated spots usually locate at the saddle points of the surface where

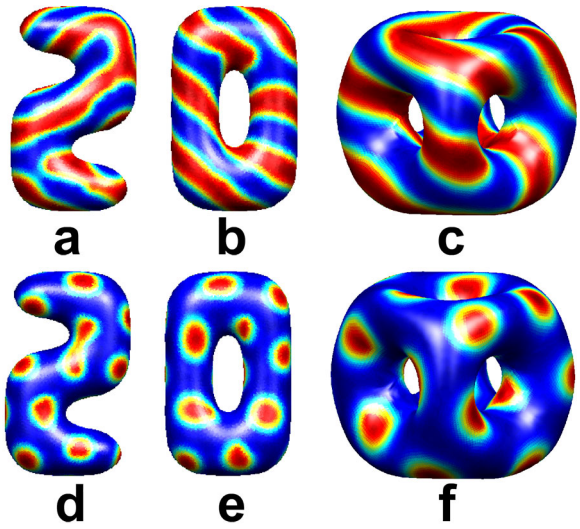

Fig. 7. The striped and spotted patterns of diblock copolymers on three different closed surfaces. The first two columns represent the number "2" and "0" with genus 0 and 1, respectively. The third column is a genus-5 cube frame. Red is for A blocks and Blue for B blocks. Parameter setting: $N = 50$, $\chi N = 13$ and $f = 0.5$ for the upper row, and $N = 50$, $\chi N = 13$ and $f = 0.3$ for the lower row.

Table 2. The information about the triangulations of the shapes of "2", "0" and a genus-5 cube frame (CF). N_v, N_E and N_F are the numbers of the vertices, edges and faces of the triangulations, respectively. S, V and v are the area, the volume and the reduced volume of the shape, where $v \equiv 6V\pi^{1/2}S^{-3/2}$. g is the genus of the closed surface.

	N_v	N_E	N_F	area	volume	v	genus
"2"	1474	4416	2944	1774	4119	0.59	0
"0"	1536	4608	3072	1851	4254	0.57	1
"CF"	1912	5760	3840	2192	4241	0.44	5

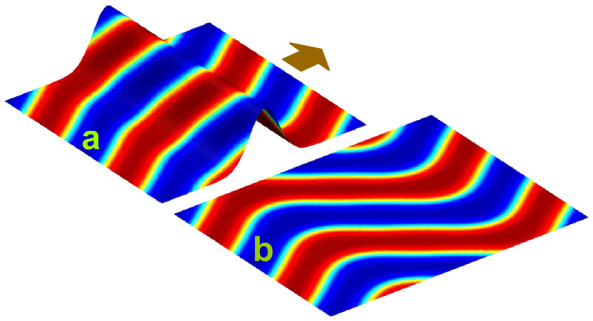

Fig. 8. (a) The striped pattern of symmetric A/B copolymers on a quasi-flat surface with a bump described by eq. (24). (b) The striped pattern of symmetric A/B copolymers on a flat surface that is isometrically equivalent to that of (a). Note that in these calculations, the surface was discretized using a quadrangular mesh and periodic boundary conditions were employed.

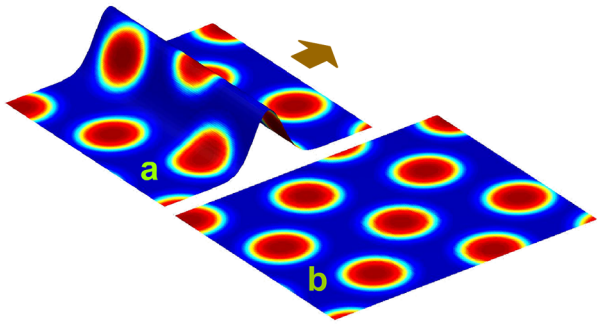

Fig. 9. (a) The spotted pattern of asymmetric A/B copolymers ($f = 0.3$) on a quasi-flat surface with a bump described by eq. (24). (b) The spotted pattern of asymmetric A/B copolymers ($f = 0.3$) on a flat surface that is isometrically equivalent to that of (a). Note that in these calculations, the surface was discretized using a quadrangular mesh and periodic boundary conditions were employed.

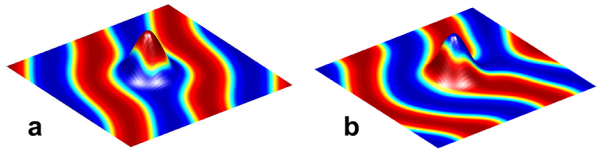

Fig. 10. (a) A striped pattern formed by symmetric A/B copolymers on a quasi-flat surface with a small hill (peak) described by eq. (25). A spotted A-dominant domain is formed at the hill's peak. (b) Another striped pattern form on the same surface. No spotted domain is formed, but this pattern has a higher free energy. Note that in these calculations, the surface was discretized using a quadrangular mesh and periodic boundary conditions were employed.

the Gaussian curvature is negative (see the spotted patterns on the number of "2" in fig. 7). These two observations may imply that the spotted phase favors the positive Gaussian curvature while the striped phase prefers the negative Gaussian curvature. Although these findings are consistent with the theoretical prediction made in sect. 2.1, the above results are still obscured and, at the same time, the effects of the mean curvature on the morphologies still can not be clarified merely by these calculations. Therefore, more calculations on quasi-flat surfaces will be given in the next subsection.

3.3 Gaussian chains can only "feel" the intrinsic curvature

In fig. 8 and fig. 9, we place AB diblocks on a bumping surface [34] that can be described by the height function

$$h(x,y) = be^{-\frac{(x-x_0)^2}{a^2}}, \tag{24}$$

where the parameters b and a control the height and the width of the bump, respectively. This surface will be of zero Gaussian curvature everywhere but with a non-vanishing mean curvature. Note that Gaussian curvature is the intrinsic curvature of the surface since it is invariant under isometric transformations while mean curvature is extrinsic. As can be seen from fig. 8 and fig. 9, the Gaussian diblock chains act as if there were no such bump. Therefore, in this example we have demonstrated that the Gaussian chains would not respond to the mean curvature: as long as the surfaces are isometrically equivalent, then there is no difference for Gaussian chains. In the current case, the bumping surface and the flat surface are the isometrically equivalent. Note that, unlike Gaussian chains, the semiflexible chains can "feel" the mean curvature of the surface according to our recent work [35]. Specifically, there will be an extra term related with the normal curvature of the surface and the orientation of the chain segment in the diffusion equation of the propagator of semiflexible polymers.

We also place the same diblock copolymers on a surface with the height function

$$h(x,y) = be^{-\frac{(x-x_0)^2+(y-y_0)^2}{a^2}}. \tag{25}$$

Now, Gaussian curvature would not be zero everywhere anymore. As discussed in sect. 2.1 the spotted phase would be dragged to the peak by an extra field $Na^2Kr^2(\nabla^2_{fl}q)/24q$, where the Gaussian curvature is positive. Figure 10 and fig. 11 both support this prediction. In partic-

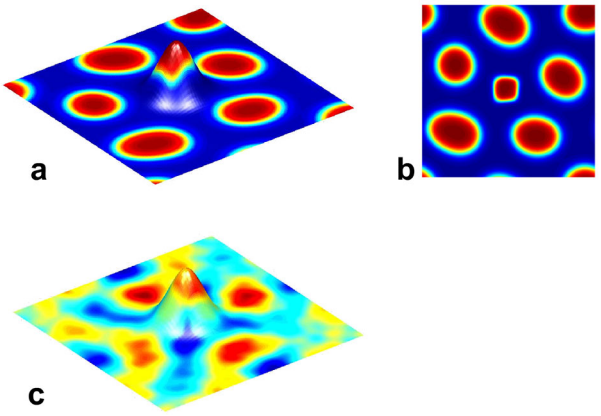

Fig. 11. (a) A spotted pattern formed by asymmetric A/B copolymers ($f = 0.3$) on a quasi-flat surface with a small hill (peak) described by eq. (25). (b) Top view of the same pattern. (c) An "averaged" spotted pattern of asymmetric A/B copolymers ($f = 0.3$) obtained by averaging 40 calculated patterns, *i.e.* $\langle\phi\rangle = \sum_{k=1}^{40} \phi_k/40$, with different random initial fields.

ular, the lamellar stripes try to avoid the peak and a spot is formed at the peak of the surface in fig. 10a. But it is not always the case for striped patterns which can be seen from fig. 10b, where no spotted phase domain forms on the peak even though the stripes attempt to circumnavigate it. For the spotted phase ($f = 0.3$), there is a clear tendency for spots to stay on the positive-Gaussian-curvature peak (fig. 11). The above observation might explain some of the patterns formed on a non-planar surface in experiments [27], though their focus was not on the Gaussian-curvature effect. In addition, many experiments [36,37] have been devoted to studying the systems of polymers on (or grafted to) nano-particles, but it is still extremely difficult to make comparisons of our simulation results to those experiments directly at the moment.

4 Conclusions

This article is mainly devoted to developing a general theoretical framework for the study of the self-assembly of block copolymers confined to curved surfaces based on the self-consistent field theory (SCFT). The numerical implementations are also given accordingly. A sophisticated numerical method for SCFT on general curved surfaces has been shown to be very powerful in calculating the intricate patterns of copolymers on different curved surfaces. A simpler implementation of SCFT on quasi-flat surfaces is also presented, which should be easier for other researchers to follow. The effects of curved surfaces on Gaussian chains are specially discussed in theory. It is predicted that the Gaussian chains can only "feel" the intrinsic curvature (Gaussian curvature). Mathematically, the self-assembly of Gaussian chains on two isometrically equivalent surfaces will be exactly the same even though the two surfaces may have different local mean curvatures. The theoretical prediction for Gaussian block copolymers is consistent with our curved-surface SCFT (CSSCFT) simulations using the numerical implementations for quasi-flat surface. In particular, it is found that the spotted patterns prefer to stay at surface locations with positive Gaussian curvature.

However, the curvature effects of curved surfaces on the self-assembly of block copolymers have been only studied qualitatively by CSSCFT in the current work and more works along this line will be presented in our future publications. In our recent work [35], we have shown, in theory, that semiflexible chains are sensitive to both intrinsic and extrinsic curvatures of the surface and it will be extremely interesting to see how the rod-coil copolymers [38] respond to curved surfaces. It is generally believed that the spectral method is more precise than the real-space method of SCFT and, therefore, it is also desirable to develop a spectral method for curved-surface SCFT of block copolymers. One possible proposal is to span the self-consistent fields on the Laplace-Beltrami eigenfunctions [39] as basis functions to formulate the spectral method for CS-SCFT. We will seriously consider this proposal in our future works.

Further, a surface without thickness only exists in an ideal world and the Gaussian chain might detect the extrinsic curvature of a surface due to the extra freedom introduced by the thickness of the surface. Luckily, it is straightforward to extend our CSSCFT to consider the thickness of the surface by simply stacking together, along the normal direction, several curved-surface meshes with the same topology but with slightly different sizes to form a discrete surface with thickness.

We thank the National Basic Research Program of China (Grant No. 2011CB605700) and NSFC (Grants No. 20874019, 20990231, and 21104010) for financial support.

References

1. H.Q. Xiang, K. Shin, T. Kim, S. Moon, T.J. McCarthy, T.P. Russell, J. Polym. Sci. Part B **43**, 3377 (2005).
2. B. Yu, P.C. Sun, T.H. Chen, Q.H. Jin, D.T. Ding, B.H. Li, A.-C. Shi, Phys. Rev. Lett. **96**, 138306 (2006).
3. Y.Y. Wu, G.S. Cheng, K. Katsov, S.W. Sides, J.F. Wang, J. Tang, G.H. Fredrickson, M. Moskovits, G.D. Stucky, Nat. Mater. **3**, 816 (2004).
4. H. Xiang, K. Shin, T. Kim, S.I. Moon, T.J. McCarthy, T.P. Russell, Macromolecules **38**, 1055 (2005).
5. W. Li, R.A. Wickham, Macromolecules **39**, 8492 (2006).
6. P. Chen, H.J. Liang, A.-C. Shi, Macromolecules **40**, 7329 (2007).
7. M. Ma, E.L. Thomas, G.C. Rutledge, B. Yu, B.H. Li, Q.H. Jin, D.T. Ding, A.-C. Shi, Macromolecules **43**, 3061 (2010).
8. P. Chi, Z. Wang, B.H. Li, A.-C. Shi, Langmuir **27**, 11683 (2011).
9. G.H. Griffiths, B. Vorselaars, M.W. Matsen, Macromolecules **44**, 3649 (2011).
10. B. Yu, B.H. Li, Q.H. Jin, D.T. Ding, A.-C. Shi, Macromolecules **40**, 9133 (2007).
11. B. Yu, B.H. Li, Q.H. Jin, D.T. Ding, A.-C. Shi, Soft Matter **7**, 10227 (2011).

12. H. Xu, J.F. Li, H.D. Zhang, Y.L. Yang, Acta Polym. Sin. **5**, 548 (2011).
13. P. Tang, F. Qiu, H.D. Zhang, Y.L. Yang, Phys. Rev. E **72**, 016710 (2005).
14. J.F. Li, J. Fan, H.D. Zhang, F. Qiu, P. Tang, Y.L. Yang, Eur. Phys. J. E **20**, 449 (2006).
15. T.L. Chantawansri *et al.*, Phys. Rev. E **75**, 031802 (2007).
16. G.H. Fredrickson, *The Equilibrium Theory of Inhomogeneous Polymers* (Clarendon Press, Oxford, 2006).
17. M.W. Matsen, M. Schick, Phys. Rev. Lett. **72**, 2660 (1994).
18. P. Tang, F. Qiu, H.D. Zhang, Y.L. Yang, Phys. Rev. E **69**, 031803 (2004).
19. P. Tang, F. Qiu, H.D. Zhang, Y.L. Yang, J. Phys. Chem. B **108**, 8434 (2004).
20. Z.J. Guo *et al.*, Phys. Rev. Lett. **101**, 028301 (2008).
21. F. Drolet, G.H. Fredrickson, Phys. Rev. Lett. **83**, 4317 (1999).
22. F. Drolet, G.H. Fredrickson, Macromolecules **34**, 5317 (2001).
23. E. Helfand, J. Chem. Phys. **62**, 999 (1975).
24. W.H. Press, B.P. Flannery, S.A. Teukolsky, W.T. Vetterling, *Numerical Recipes* (Cambridge University Press, Cambridge, 1989).
25. J.U. Kim, M.W. Matsen, Macromolecules **41**, 4435 (2008).
26. B. Vorselaars, J.U. Kim, T.L. Chantawansri, G.H. Fredrickson, M.W. Matsen, Soft Matter **7**, 5128 (2011).
27. E. Sivaniah, J. Genzer, A. Hexemer, E.J. Kramer, M.L. Xiang, X.F. Li, C.K. Ober, S. Magonov, Macromolecules **41**, 9940 (2008).
28. H. Kleinert, *Path Integrals in Quantum Mechanics, Statistics, Polymer Physics, and Financial Markets*, 4th edition (World Scientific, Hackensack, NJ, 2006).
29. M. Berger, *A Panoramic View of Riemannian Geometry* (Springer-Verlag, Berlin, 2004).
30. K.A. Brakke, Exp. Math. **1**, 141 (1992).
31. J.F. Li, H.D. Zhang, F. Qiu, J. Phys. Chem. B **117**, 843 (2013).
32. M. Meyer *et al.*, *VisMath Proceedings* (Berlin, 2002).
33. J. Sherman, W.J. Morrison, Ann. Math. Stat. **20**, 621 (1949).
34. A. Hexemer, V. Vitelli, E.J. Kramer, G.H. Fredrickson, Phys. Rev. E **76**, (2007).
35. Q. Liang, J.F. Li, P.W. Zhang, J.Z.Y. Chen, J. Chem. Phys. **138**, 244910 (2013).
36. B. Zhao L. Zhu, Macromolecules **42**, 9369 (2009).
37. R.P. Carney, G.A. DeVries, C. Dubois, H. Kim, J.Y. Kim C. Singh, P.K. Ghorai, J.B. Tracy, R.L. Stiles, R.W. Murray, S.C. Glotzer, F. Stellacci, J. Am. Chem. Soc. **130**, 798 (2008).
38. W.D. Song, P. Tang, F. Qiu, Y.L. Yang, A.-C. Shi, J. Phys. Chem. B **115**, 8390 (2011).
39. B. Vallet, B. Levy, Comput. Graph. Forum **27**, 251 (2008).